EVOLUTION OF RAPID, SHEAR-GENERATED GUSTS

Ingrid Neunaber
FLOW, Department of Engineering Mechanics
KTH Royal Institute of Technology
Stockholm, Sweden
neunaber@kth.se

Martin Obligado
Centrale Lille Institut
Institut Universitaire de France
Lille, France
martin.obligado@centralelille.fr

Caroline Braud
LHEEA Laboratory
Nantes Université, Ecole Centrale Nantes, CNRS
Nantes, France
caroline.braud@ec-nantes.fr

ABSTRACT

We present a detailed study of the turbulence generated by the Chopper, a gust generator installed at the wind tunnel of Centrale Nantes in France. The Chopper, a rotating bar that cuts through the inlet of the test section, generates strong, sudden, turbulent flow disturbances. The impact of the inlet wind speed and the rotational speed of the Chopper blade on the gust shape and turbulence are investigated by means of hot-wire measurements. While the average gust velocity is constant up to a blade passing frequency of 0.2 Hz, it increases for higher frequencies and seems to stabilize above 1.0 Hz. The gust length was found to be inversely proportional to the blade rotational frequency. The energy spectra show a clear inertial subrange with a -5/3 power law decay, and in accordance with the average gust velocity, we identify two shifted inertial ranges, one for blade passing frequencies up to 0.2 Hz and one for blade passing frequencies above 0.4 Hz. The intermittency parameter, that quantifies the rate of degaussianisation of the streamwise velocity derivative in the inertial range, shows a clear difference between non-turbulent and turbulent inflow, but it is independent of the blade passing frequency.

INTRODUCTION

Atmospheric gusts, i.e., (very) strong, (very) sudden changes of the flow velocity, can cause problems in many applications, e.g., performance of unmanned aerial vehicles (Stutz *et al.*, 2023), aircraft safety, or wind energy (e.g., Kosović *et al.* (2025)).

Therefore, it is of interest to model sudden, strong variations of the inflow under controlled conditions in wind tunnels. For this, various systems have been envisaged, of which a few will be briefly discussed in the following.

Transverse gusts can be modelled by adding a cross-flow that is perpendicular to the stream-wise direction. The cross-flow can either pass from an inlet through the test section to an outlet (e.g., Corkery *et al.* (2018) in a water channel and Poudel *et al.* (2018) in a wind tunnel), or from an inlet onto the opposite side of the test section, in which case it would model a thunderstorm downburst, e.g., Zhang *et al.* (2015).

For the generation of stream-wise gusts, different methods have been tested. For example, Horlock (1974) presents a wind tunnel with test section walls that are flexible and can be controlled to produce sinusoidal transverse and streamwise gusts. Through blockage modulation at the end of the test section of an open jet facility, Greenblatt (2016) achieves flow variations. These approaches all focus on variations of the velocity while keeping the turbulence intensity low. Active devices at the inlet of the wind tunnel, such as rotating slotted cylinders (Tang *et al.*, 1996) or a pitching and plunging airfoil (Wei *et al.*, 2019a) can generate periodic gusts. Alternatively, an array of oscillating 2D airfoils at the inlet of the wind tunnel can be used (Wester *et al.*, 2018; Wei *et al.*, 2019b). In contrast, active grids, originally introduced by Makita (1991), are powerful tools to generate different types of turbulent inflows (Bodenschatz *et al.*, 2014; Hearst & Lavoie, 2015; Neuhaus *et al.*, 2020), shear flows (Cekli & van de Water, 2010; Hearst & Ganapathisubramani, 2017) and gusts (Berger *et al.*, 2022). While active grids stand out due to their flexibility and available research, they are also costly and complex.

In this study, we will analyse the gusts produced by yet another device, the *Chopper*: a rotating bar, the *Chopper blade*, that cuts through the inlet of a wind tunnel test section, cf. Figure 1. The Chopper has been introduced by Neunaber & Braud (2020*b*) and the gust shape and turbulence have been analysed for a Chopper blade width of 200 mm for one inflow velocity, $u_0 = 25\,\mathrm{ms}^{-1}$, and two different blade passing frequencies of the Chopper blade, $f_{CH} = 0.04\,\mathrm{Hz}$ and $f_{CH} = 0.4\,\mathrm{Hz}$. Note that the rotational frequency is half of the blade passing frequency. It was found that strong, sudden, turbulent gusts are produced that have a reproducible average gust shape. The turbulence within the gust shows strong features of homogeneous isotropic turbulence with an $f^{-5/3}$ decay within the inertial range of the spectrum.

In this work, we will present a new set of experiments that includes a new design of the Chopper blade and Chopper frequencies ranging from 0.02 Hz to 2 Hz.

SET-UP & METHODOLOGY

The experiments were carried out in the aerodynamic wind tunnel at the LHEEA laboratory at Centrale Nantes in

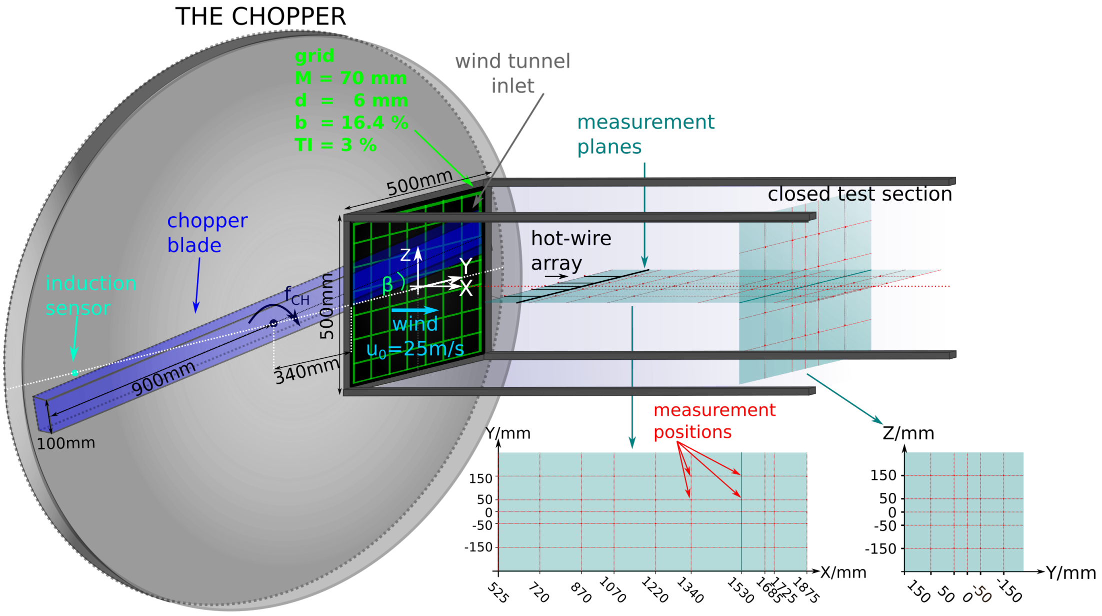

Figure 1. The Chopper consists of a rotating bar, the Chopper blade, that cuts through the inlet of the test section. Upstream of the Chopper blade, a grid can be installed to add background turbulence to the flow. The flow is scanned with an array of five hot-wire probes. A horizontal and a vertical plane are investigated.

France. It has an inlet of 500 mm × 500 mm and a test section length of 2300 mm. Maximum velocities of 40 ms^{-1} could be reached at the time the experiments were carried out.

As detailed in Figure 1, the Chopper is installed at the inlet of the test section. Its position is captured with an induction sensor when it is passing through the center of the inlet. The Chopper blade used here had a width of 100 mm.

Experiments were carried out both in the low-turbulent flow of the wind tunnel (turbulence intensity $TI \approx 0.3\%$ for an empty test section) and with a regular square grid installed upstream of the Chopper. The grid has a mesh width of $M = 70$ mm and a bar width of $b = 6$ mm, and it was installed to create turbulent background flow that evolves alongside the gust. At $x = 1585$ m, $TI \approx 3.0\%$, cf., Neunaber & Braud (2020*a*).

The inflow velocity u_0 is defined here as the velocity of the empty inlet (i.e., the Chopper blade is not blocking it) at 1530 mm downstream for both low-turbulent and turbulent inflow.

An array of 5 single hot-wires was traversed downstream in the test section. The centerline hot-wire was operated by a Disa 55M01 main unit and standard bridge, while the remaining four wires where operated using MiniCTA modules of type 54T30 from Dantec Dynamics that have a lower temporal resolution of about 10 kHz. The sampling frequency was set to $f_s = 100$ kHz and a hardware lowpass filter was set at $f_{LP} = 40$ kHz. To reduce noise from the anemometers at high frequencies, the data was additionally filtered at 20 kHz with a seventh order Butterworth filter. Depending on the Chopper frequency, the acquisition time was between 120 s and 600 s to ensure that a sufficient amount of gusts was captured. The wires were calibrated frequently using a Disa calibrator of the type 55D45 with a nozzle of 60 mm^2, and temperature correction according to Hultmark & Smits (2010) was applied.

For $u_0 = 25\,\mathrm{ms}^{-1}$ and $f_{CH} = 0.04$ Hz and 0.4 Hz, a horizontal plane and a vertical plane at 1530 mm were scanned. The exact measurement positions are presented in Figure 1. Chopper frequencies f_{CH} between 0.02 Hz and 2 Hz were additionally investigated for an inflow velocity of 25 ms^{-1} at 1530 mm downstream.

RESULTS

In the following, we will focus on the variation of the gust shape and turbulence with different Chopper frequencies at the centerline at $x = 1530$ mm at an inflow velocity of $u_0 = 25\,\mathrm{ms}^{-1}$.

In Figure 2, the normalized variation of the mean gust shape, i.e., an average over all gusts of a respective time series, cf. Neunaber & Braud (2020*b*), is shown for different Chopper frequencies both for the no-grid case (Figure 2a) and the grid case (Figure 2b) at the centerline 1530 mm downstream. The inflow velocity was $u_0 = 25\,\mathrm{ms}^{-1}$. The gusts are plotted with respect to the Chopper blade angle β, cf., Figure 1, and the blockage induced by the Chopper blade is indicated.

For low f_{CH}, the gust shape is determined by a small overshoot and a blockage-induced strong velocity deficit. With increasing f_{CH}, however, a transition to a gust with two overshoots and little velocity deficit is observed. At the measurement position, the gusts are detected later with respect to the blade position, indicating that the passing of the blade happens faster than the flow can transport the gust downstream. The impact of the added inflow turbulence on the gust consists mainly of a reduction in the gust amplitude, cf., Figure 2b).

To compare the gusts in a more quantitative manner, Figure 3 shows the mean gust velocities, defined as the average velocity of the mean gust (cf., Figure 2), and the mean gust duration. The mean gust duration is estimated by calculating the variance over bins of 500 samples length for each gust in a time series, taking the interval in which the variance exceeds a threshold of 1 $\mathrm{m}^2\mathrm{s}^{-2}$ as gust duration, and averaging over the results for all gusts of a time series. This method also allows us to include error bars that show the standard deviation of the estimates of a time series. The threshold is chosen so that it is applicable both for the low-turbulent and turbulent inflows. The mean gust velocity is constant for $0.01\,\mathrm{Hz} \leq f_{CH} \leq 0.20\,\mathrm{Hz}$, increases for $0.2\,\mathrm{Hz} \leq f_{CH} \leq 1.0\,\mathrm{Hz}$, and seems to saturate for $f_{CH} \geq 1.0\,\mathrm{Hz}$. The mean gust duration l decays according

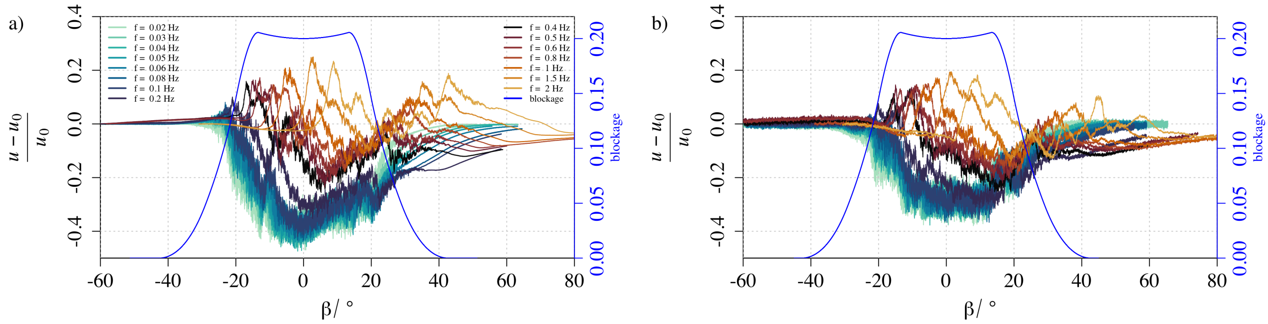

Figure 2. Mean gust shape plotted over Chopper angle for various Chopper frequencies for a) low-turbulent inflow, and b) turbulent inflow (grid installed) at $u_0 = 25\,\mathrm{ms}^{-1}$ and $x = 1530$ mm, which is equal to 15.3 Chopper blade widths.

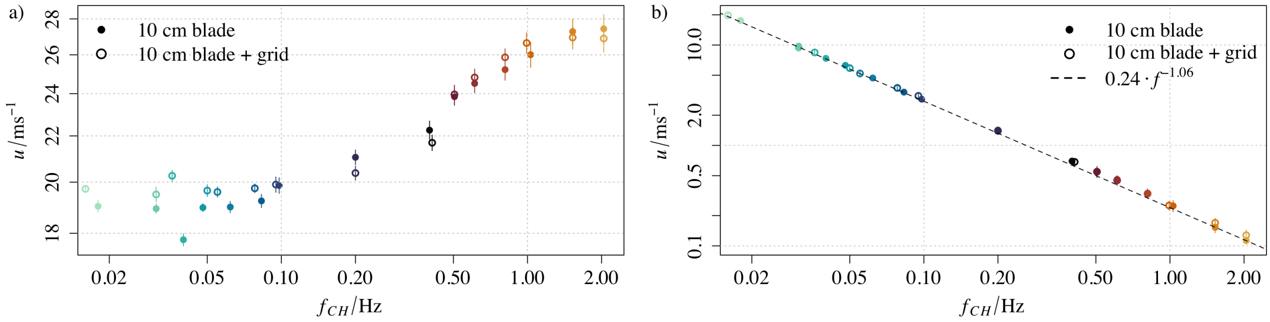

Figure 3. a) Mean gust velocity, and b) mean gust duration in dependence of the Chopper frequency at $u_0 = 25\,\mathrm{ms}^{-1}$ and $x = 1530$ mm, which is equal to 15.3 Chopper blade widths. Error bars represent the standard deviations of the gust velocities and durations of all gusts of a time series.

to $l \propto f_{CH}^{-1.06}$ despite the change in behaviour that is observed both from the mean gust shape and the mean gust velocity with increasing f_{CH}. The turbulent inflow only has a small impact on the mean gust velocity and duration.

Figure 4 shows the energy spectra $E(f)$ of the whole time series for the different Chopper frequencies at $u_0 = 25\,\mathrm{ms}^{-1}$ at the centerline 1530 mm downstream. As already reported in Neunaber & Braud (2020*b*) for $f_{CH} = 0.04$ Hz and $f_{CH} = 0.4$ Hz, the Chopper frequency and its harmonics can clearly be distinguished by peaks in the spectra. At large scales, the spectra are otherwise flat, and the inertial range extends approximately over 2 orders of magnitude, where it follows an $f^{-5/3}$ decay. The transition of the gust behavior from low to high Chopper frequencies is reflected also here through slight changes in the inertial range. The turbulent inflow does not have a major impact on the energy spectra.

To further investigate the small-scale turbulence within the gusts, next, we are investigating the Castaing parameter

$$\lambda^2(\tau) = \frac{\ln F(\delta u_\tau(t)/3)}{4}, \qquad (1)$$

that characterizes the heavy-tails of the probability density functions of velocity increments $\delta u_\tau(t) = u(t+\tau) - u(t)$ at time scales τ by means of their flatness F (Castaing *et al.*, 1990; Chilla *et al.*, 1996). Note that we use the description in time while the original framework is derived based on spatial scales. If $\lambda^2 \approx 0$, the probability density function of velocity increments at the respective time scale are Gaussian, whereas $\lambda^2 > 0$ indicates the presence of internal intermittency through heavy-tailed probability density function of velocity increments. As we are interested in the evolution of $\lambda^2(\tau)$ for the small-scale turbulence within the gusts, for this respective analysis, we subtract the average gust shape from each gust and run the analysis only on the turbulence within the gust (cf., Neunaber & Braud (2020*b*) for details on the triple-decomposition applied here). The evolution of $\lambda^2(\tau)$ averaged over all gusts of a respective time series is plotted in figure 5 for the different blade passing frequencies and for low-turbulent and turbulent inflow. For all cases, we observe that λ^2 follows a power law decay for time scales between $10^{-4} < \tau < 10^{-2}$. Such time scales, as predicted by the theory of Castaing *et al.* (1990), lie within the inertial range of turbulence. For $\tau > 10^{-2}$, λ^2 is constant and close to 0, albeit a bit larger for lower blade passing frequencies.

To further elucidate the turbulence features within the gusts, we finally calculate the intermittency parameter μ, that further characterizes the deviation of the probability density functions of velocity increments from a Gaussian distribution within the inertial range. It was introduced by Kolmogorov (1962) to take into account the scale dependence of the energy fluctuations in the scaling of the structure functions $\langle(\delta u_\tau)^n\rangle \propto \tau^{\zeta_n}$,

$$\zeta_n = \frac{n}{3} - \mu\frac{n(n-3)}{18}. \qquad (2)$$

As λ^2 is estimated based on the flatness of the velocity increments, which is the fourth order structure function divided by the second order structure function, applying the scaling from equation 2 allows us to estimate μ through fitting

$$\lambda^2 = \lambda_0^2 + \frac{\mu}{9}\ln\tau, \qquad (3)$$

where λ_0^2 is a constant encasing flow properties (Morales *et al.*, 2012; Neunaber, 2019; Schmitt *et al.*, 2026).

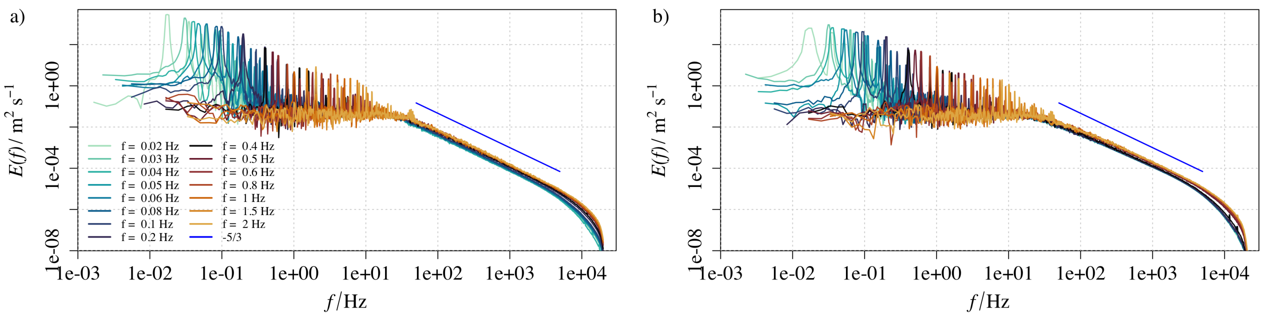

Figure 4. Spectra of the velocity time series for various Chopper frequencies for a) low-turbulent inflow, and b) turbulent inflow (grid installed) at $u_0 = 25\,\mathrm{ms}^{-1}$ and $x = 1530$ mm, which is equal to 15.3 Chopper blade widths.

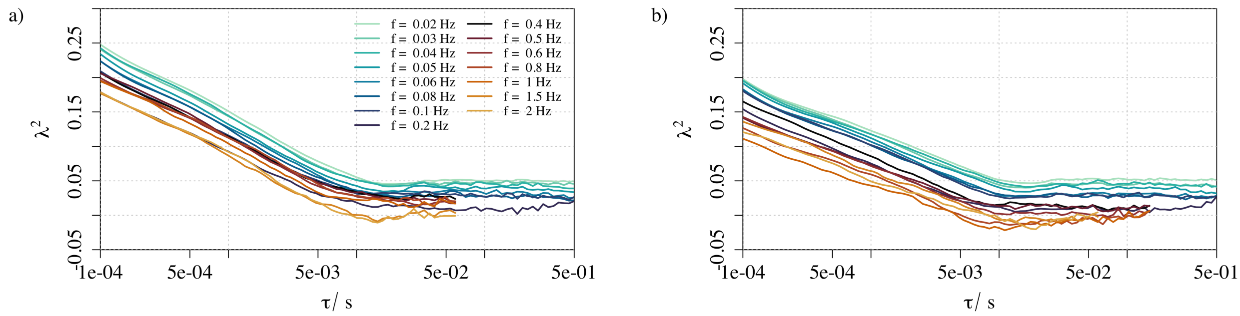

Figure 5. Evolution of the Castaing parameter λ^2 for various Chopper frequencies for a) low-turbulent inflow, and b) turbulent inflow (grid installed) at $u_0 = 25\,\mathrm{ms}^{-1}$ and $x = 1530$ mm, which is equal to 15.3 Chopper blade widths.

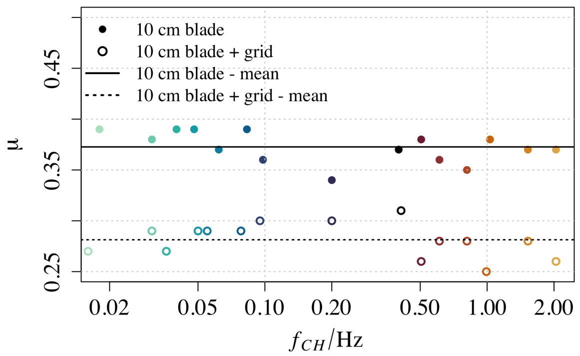

Figure 6. Intermittency factor μ in dependence of the Chopper frequency at $u_0 = 25\,\mathrm{ms}^{-1}$ and $x = 1530$ mm, which is equal to 15.3 Chopper blade widths.

The results of this analysis can be found in figure 6. While no trends can be seen for an evolution of μ in dependence of the Chopper frequency, there is a clear difference between the low-turbulent and turbulent inflow. In the case of low-turbulent inflow, the average intermittency parameter is $\bar{\mu} \approx 0.37$, whereas it is $\bar{\mu} \approx 0.28$ for the turbulent inflow case. While both values are within the reported range for homogeneous isotropic turbulence at moderate Taylor Reynolds numbers, cf., Schmitt *et al.* (2026) and references therein, this clear difference demonstrates that this analysis allows us to identify differences in the small scale turbulence between low-turbulent and turbulent inflow that remained hidden with standard evaluation methods.

CONCLUSIONS

First results from an extensive campaign studying the gusts produced by the Chopper were presented. We find that the average gust has a decreasing amplitude with increasing Chopper frequency and that the duration decreases according to $l \propto f_{CH}^{-1}$. The mean gust velocity seems to stabilize both for $f_{CH} \leq 0.2\,\mathrm{Hz}$ and for $f_{CH} \geq 1.0\,\mathrm{Hz}$ with a transition in between, that is also present in the spectra. The impact of a turbulent inflow on the results is small when taking into account standard analysis methods. However, through an analysis of the small scale turbulence within the gust by means of the evolution of the shape parameter $\lambda^2(\tau)$ in dependence of the scale τ, and the intermittency parameter μ, we showed that, while the gust turbulence exhibits values typical for homogeneous, isotropic turbulence for both low-turbulent and turbulent inflow, these values differ. This is an indication that the inflow turbulence affects the small-scale turbulence within the gust, which warrants further investigations.

Next evaluation steps will be focusing both on the gust shape at different span-wise positions and at different inflow velocities, and on investigating the turbulence statistics by means of gust turbulence intensity, and higher-order two-point statistics.

REFERENCES

Berger, F., Neuhaus, L., Onnen, D., Hölling, M., Schepers, G. & Kühn, M. 2022 Experimental analysis of the dynamic inflow effect due to coherent gusts. *Wind Energy Sci.* **7** (5), 1827–1846.

Bodenschatz, E., Bewley, G. P., Nobach, H., Sinhuber, M. & Xu, H. 2014 Variable density turbulence tunnel facility. *Rev. Sci. Instrum.* **85** (9), 093908.

Castaing, B., Gagne, Y. & Hopfinger, E. J. 1990 Velocity probability density functions of high reynolds number turbulence. *Physica D* **46** (2), 177–200.

Cekli, H. E. & van de Water, W. 2010 Tailoring turbulence with an active grid. *Exp. Fluids* **49**, 409–416.

Chilla, F., Peinke, J. & Castaing, B. 1996 Multiplicative process in turbulent velocity statistics: A simplified analysis. *J. Phys. II Fr.* **6** (4), 455–460.

Corkery, S. J., Babinsky, H. & Harvey, J. 2018 Response of a flat plate wing to a transverse gust at low reynolds numbers. *AIAA Aerosp. Sci. Meet.* **210059**.

Greenblatt, D. 2016 Unsteady low-speed wind tunnels. *AIAA J.* **54** (6).

Hearst, R. J. & Ganapathisubramani, B. 2017 Tailoring incoming shear and turbulence profiles for lab-scale wind turbines. *Wind Energy* **20**, 2021–2035.

Hearst, R. J. & Lavoie, P. 2015 The effect of active grid initial conditions on high reynolds number turbulence. *Exp. Fluids* **56** (185).

Horlock, J. H. 1974 An unsteady flow wind tunnel. *Aeronaut. Q.* **25**, 81–90.

Hultmark, M. & Smits, A. J. 2010 Temperature corrections for constant temperature and constant current hot-wire anemometers. *Meas. Sci. Technol.* **21**, 105404.

Kolmogorov, A. N. 1962 A refinement of previous hypotheses concerning the local structure of turbulence in a viscous incompressible fluid at high reynolds number. *J. Fluid Mech.* **13** (1), 82–85.

Kosović, B., Basu, S., Berg, J., Berg, L. K., Haupt, S. E., Larsén, X. G., Peinke, J., Stevens, R. J. A. M., Veers, P. & Watson, S. 2025 Impact of atmospheric turbulence on performance and loads of wind turbines: Knowledge gaps and research challenges. *Wind Energy Sci. Discuss.* **2025**, 1–67.

Makita, H. 1991 Realization of a large-scale turbulence field in a small wind tunnel. *Fluid Dyn. Res.* **8**, 53–64.

Morales, A., Wächter, M. & Peinke, J. 2012 Characterization of wind turbulence by higher-order statistics. *Wind Energy* **15** (3), 391–406.

Neuhaus, Lars, Hölling, Michael, Bos, Wouter J. T. & Peinke, Joachim 2020 Generation of atmospheric turbulence with unprecedentedly large reynolds number in a wind tunnel. *Phys. Rev. Lett.* **125** (15), 154503.

Neunaber, I. 2019 Stochastic investigation of the evolution of small-scale turbulence in the wake of a wind turbine exposed to different inflow conditions. PhD thesis, Carl von Ossietzky Universität Oldenburg.

Neunaber, Ingrid & Braud, Caroline 2020*a* Aerodynamic behavior of an airfoil under extreme wind conditions. *J. Phys. Conf. Ser.* **1618** (3), 032035.

Neunaber, I. & Braud, C. 2020*b* First characterization of a new perturbation system for gust generation: the chopper. *Wind Energy Sci.* **5** (2), 759–773.

Poudel, N., Yu, M., Smith, Z. F. & Hrynuk, J. T. 2018 A combined experimental and computational study of a vertical gust generator in a wind tunnel. *AIAA Scitech Forum* .

Schmitt, F. H., Köhne, F., Peinke, J. & Obligado, M. 2026 On small-scale intermittency for general turbulence. *J. Phys. Conf. Ser.* **3173** (1), 012024.

Stutz, Colin M., Hrynuk, John T. & Bohl, Douglas G. 2023 Effects of vehicle dynamics on small uas-gust encounters. *Aerosp. Sci. Technol.* **142**, 108679.

Tang, D. M., Paul, G. A. & Dowell, E. H. 1996 Experiments and analysis for a gust generator in a wind tunnel. *J. Aircr.* **33** (1).

Wei, N. J., Kissing, J. & Tropea, C. 2019b Generation of periodic gusts with a pitching and plunging airfoil. *Exp. Fluids* **60** (166).

Wei, N. J., Kissing, J., Wester, T. T. B., Wegt, S., Schiffmann, K., Jakirlic, S., Hölling, M., Peinke, J. & Tropea, C. 2019a Insights into the periodic gust response of airfoils. *J. Fluid Mech.* **876**, 237–263.

Wester, T. T. B., Kampers, G., Gülker, G., Peinke, J., Cordes, U., Tropea, C. & Hölling, M. 2018 High speed piv measurements of an adaptive camber airfoil under highly gusty inflow conditions. *J. Phys. Conf. Ser.* **1037**, 072007.

Zhang, Y., Sarkar, P. P. & Hu, H. 2015 An experimental investigation on the characteristics of fluid–structure interactions of a wind turbine model sited in microburst-like winds. *J. Fluids Struct.* **57**, 206–218.